

CMV-induced Embryonic Mouse Organ of Corti Dysplasia: Network Architecture of Dysfunctional Lateral Inhibition

Michael Melnick and Tina Jaskoll*

Background: Congenital cytomegalovirus infection is the major nongenetic cause of sensorineural hearing loss at birth and beyond. Among other pathologies, there is a striking dysplasia/hyperplasia of organ of Corti hair and supporting cells. **Methods:** Using an in vitro embryonic mouse model of cytomegalovirus-induced cochlear teratogenesis that mimics the known human pathology, and functional signaling network modeling, we tested the hypothesis that cytomegalovirus disrupts the highly ordered organ of Corti hair and supporting cells pattern by dysregulating Notch and *Fgfr3*, their cognate ligands and downstream effectors. **Results:** Several novel emergent properties of the critical lateral inhibition subnetwork became apparent. The subnetwork has classic small-world properties such as short paths between most gene pairs, few long-distance links, and considerable clustering. Concomitantly, the

calculated probability that our specific gene expression dataset is from dysplastic organs of Corti is highly significant ($p < 1 \times 10^{-12}$). Furthermore, we determined that the subnetwork has a highly heterogeneous scale-free topology in which the highly linked genes (hubs), *Notch* and *Fgfr3*, play a central role in mediating interactions among the less linked genes. **Conclusion:** This phenomenon has important biologic and therapeutic implications.

Birth Defects Research (Part A) 103:573–582, 2015.
© 2015 Wiley Periodicals, Inc.

Key words: CMV; organ of Corti; hair cells; Notch; *Fgfr3*; network architecture

Introduction

Congenital cytomegalovirus (CMV) infection is the leading cause of nongenetic sensorineural hearing loss (SNHL) in children in the United States (Fowler, 2013). Every year more than 4000 children are born in the United States who have congenital CMV-induced SNHL at birth or later in childhood (Fowler, 2013; www.cdc.gov/cmV). Morton and Nance (2006) estimate that 21% of SNHL at birth and 25% of SNHL at age 4 is caused by congenital CMV infection. Despite decades of intense efforts, a safe and effective anti-CMV vaccine is not imminent. Furthermore, there are serious concerns about the efficacy and safety of present antiviral drugs for extended use in prenatates, neonates, and infants with congenital CMV infection (Schleiss and McVoy, 2004; Andrei et al., 2008; Cheeran et al., 2009; Schleiss, 2011). Alternatively, one current cutting edge therapeutic strategy is to identify and target host signaling molecules which are essential for viral replication and/or tissue (organ) pathogenesis (Andrei et al., 2008; Schwegmann and Brombacher, 2008; Melnick et al., 2014). Indeed, CMV highly dysregulates many host genes related to development and differentiation (Melnick et al., 2006; Jaskoll et al., 2008a,b, 2010; Juranac Lisnic et al., 2013).

Recently, we presented an in vitro embryonic mouse organ model of CMV-induced cochlear teratogenesis that

mimics the known human pathology, including dysplasia of the organ of Corti, Reissner's membrane, and stria vascularis (Melnick and Jaskoll, 2013). One of the key abnormalities is hyperplasia and disorganization of hair (HC) and supporting (SC) cells in the organ of Corti (Fig. 1). Normally, the four HCs and adjacent SCs arrange themselves in a checkerboard pattern along the entire length of the cochlear duct (Kelley, 2007), mediating sensorineural hearing (Fig. 1). Through lateral inhibition (Fig. 2), the Notch and FGFR3 signaling pathways are critical to the formation of the highly ordered mosaic of HCs and SCs from an epithelial placode of prosensory cells with an inherent tendency to adopt an HC fate (Kiernan et al., 2005; Hayashi et al., 2007; Jacques et al., 2007, 2012; Doetzlhofer et al., 2009; Kelly and Chen, 2009; Murata et al., 2009, 2012; Pan et al., 2010; Kiernan, 2013).

HC differentiation upregulates the expression of two critical membrane-bound Notch ligands, Jag2 and Dll1; shortly thereafter (~ 24 hr), Notch is activated in adjacent cells, precluding HC differentiation (lateral inhibition) and permitting SC differentiation (Fig. 2). It appears that the mechanical pulling force produced by endocytosis of Notch-bound ligand drives conformational changes in Notch that permit activating proteolysis (Meloty-Kapella et al., 2012; Musse et al., 2012). Cleaved, activated Notch (aNotch) serves as a transcription factor, upregulating important Notch target effectors such as *Hes5*, an inhibitor of *Atoh1*, a protein critical for HC differentiation (Driver et al., 2013; Jahan et al., 2013). Thus, to be driven to a SC phenotype, a prosensory cell must be actively inhibited from becoming a HC (Driver et al., 2013). Furthermore, Notch also plays a key role in promoting the cell cycle withdrawal so critical to the precisely patterned cellular mosaic (Kiernan et al., 2005).

In a largely Notch-independent manner, *Fgf8-Fgfr3* signaling also regulates cell patterning (Fig. 2) through the

Laboratory Developmental Genetics, University of Southern California, Los Angeles, California.

Supported by NIH grant R21 DC010424.

*Correspondence to: Michael Melnick, Laboratory for Developmental Genetics, University of Southern California, 925 W 34th Street, DEN 4266, MC-0641, Los Angeles, CA 90089-0641. E-mail: mmelnick@usc.edu

Published online 14 July 2015 in Wiley Online Library (wileyonlinelibrary.com).
Doi: 10.1002/bdra.23386

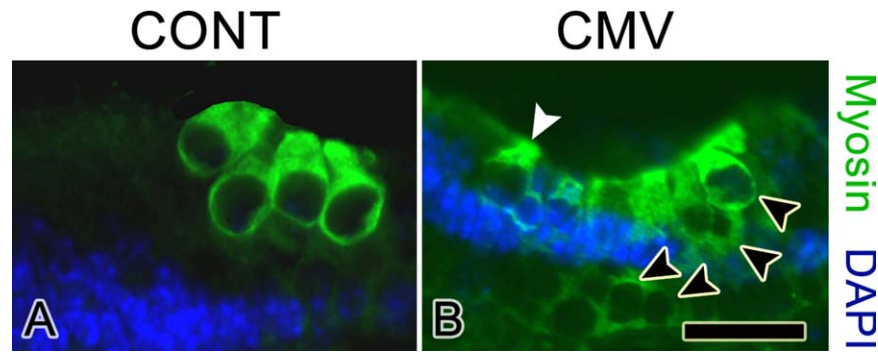


FIGURE 1. *mCMV* induces a dramatic increase in densely packed and misaligned hair cells in E15+12 cochleas. Hair cells are labeled with an antibody to myosin (myo, green); nuclei are stained with DAPI (blue). Controls (**A**) display one inner hair cell and three outer hair cells properly aligned. In contrast, *mCMV*-infected cochleas (**B**) exhibit one inner hair cell (white arrowhead) and an expanded outer hair cell population (black arrowheads) which is densely packed and disorganized. Scale bar = 30 μm .

induction of pillar SCs and the simultaneous inhibition of outer HCs in separate progenitor cells (Jacques et al., 2007; Hayashi et al., 2007; Puligilla et al., 2007). Doetzlhofer et al. (2009) present data suggesting the Fgfr and Notch signaling act redundantly. Additionally, recent studies reveal that microtubule formation is a major downstream effector of Fgfr3 signaling, and Fgfr3 loss of function impacts the formation of fluid spaces in the organ of Corti (Szarama et al., 2012).

In the present studies, combining a three-dimensional mouse model of CMV-induced cochlear teratogenesis with functional network modeling, we tested the hypothesis that CMV disrupts the highly ordered HC/SC pattern in the organ of Corti by dysregulating Notch and Fgfr3, their cognate ligands, and other downstream effectors. To wit, we present evidence that dysregulation of canonical Notch and/or Fgfr3 signaling is sufficient to account for differential quantitative expression of HC/SC developmentally critical genes in the context of CMV infection, and, consequently, the emergent histopathology.

Methods

ANIMALS

Timed pregnant inbred C57/BL6 female mice were purchased from Harlan Laboratories (Indianapolis, IN) (plug day = day 0 of gestation) and E15 embryos were harvested as previously described (Melnick et al., 2006, 2009, 2011). All protocols involving mice were approved by the Institutional Animal Care and Use Committee (USC, Los Angeles, CA).

ORGAN CULTURE

Whole inner ears were dissected from embryonic day 15 (E15) mouse fetuses and the ventral cochlear region and dorsal vestibular region were separated. Cochleas were cultured using a modified otic organ culture system first described by Van de Water and Ruben (1971) and

chemically defined BGJb medium (Invitrogen Corporation, Carlsbad, CA) supplemented with 10% fetal calf serum (FCS), 0.5 mg ascorbic acid/ml and 50 units/ml penicillin/streptomycin (Invitrogen Corporation), pH 7.2 as previously described (Melnick et al., 2006, 2011). We cultured cochlear ducts with surrounding periotic mesenchyme because prior studies have demonstrated cochlear morphogenesis and hair cell differentiation are dependent on a complex series of interactions between otic epithelia and periotic mesenchyme (e.g., Van de Water and Represa, 1991; Doetzlhofer et al., 2004; Xu et al., 2007) and *mCMV* appears to primarily infect embryonic mesenchyme (Melnick et al., 2006; Jaskoll et al., 2008a, 2008b; Melnick and Jaskoll, 2013). For *mCMV* infection, cochleas were incubated with 1×10^{-5} plaque-forming units (PFU)/ml of *lacZ*-tagged *mCMV* RM427+ in BGJb on day 0 for 24 hr and then cultured in virus-free media for a total culture period of 6 (E15 + 6) or 9 (E15 + 9) days; controls consisted of cochleas cultured in control medium for the entire period. Cochleas were collected and processed for hematoxylin and eosin histology, quantitative reverse transcriptase-polymerase chain reaction (qRT-PCR), and immunolocalization. For qRT-PCR, four to five E15 + 6 and E15 + 9 control and *mCMV*-infected cochleas were pooled, snap frozen, and stored at -80°C . For immunolocalization analyses, cochleas were fixed for 4 hr in Carnoy's fixative or overnight in 4% paraformaldehyde at 4°C , embedded in paraffin, serially sectioned and stained as previously described (Melnick et al., 2006, 2011, 2013a,b).

IMMUNOLocalIZATION

Cultured cochleas were embedded in low melting point paraplast, serially sectioned at 8 μm and immunostained essentially as previously described (Melnick et al., 2006, 2011, 2013a,b; Melnick and Jaskoll, 2013) using the following commercially available antibodies: myosin-VI (Proteus Biosciences, Inc, Ramona, CA; cat # 25-6791);

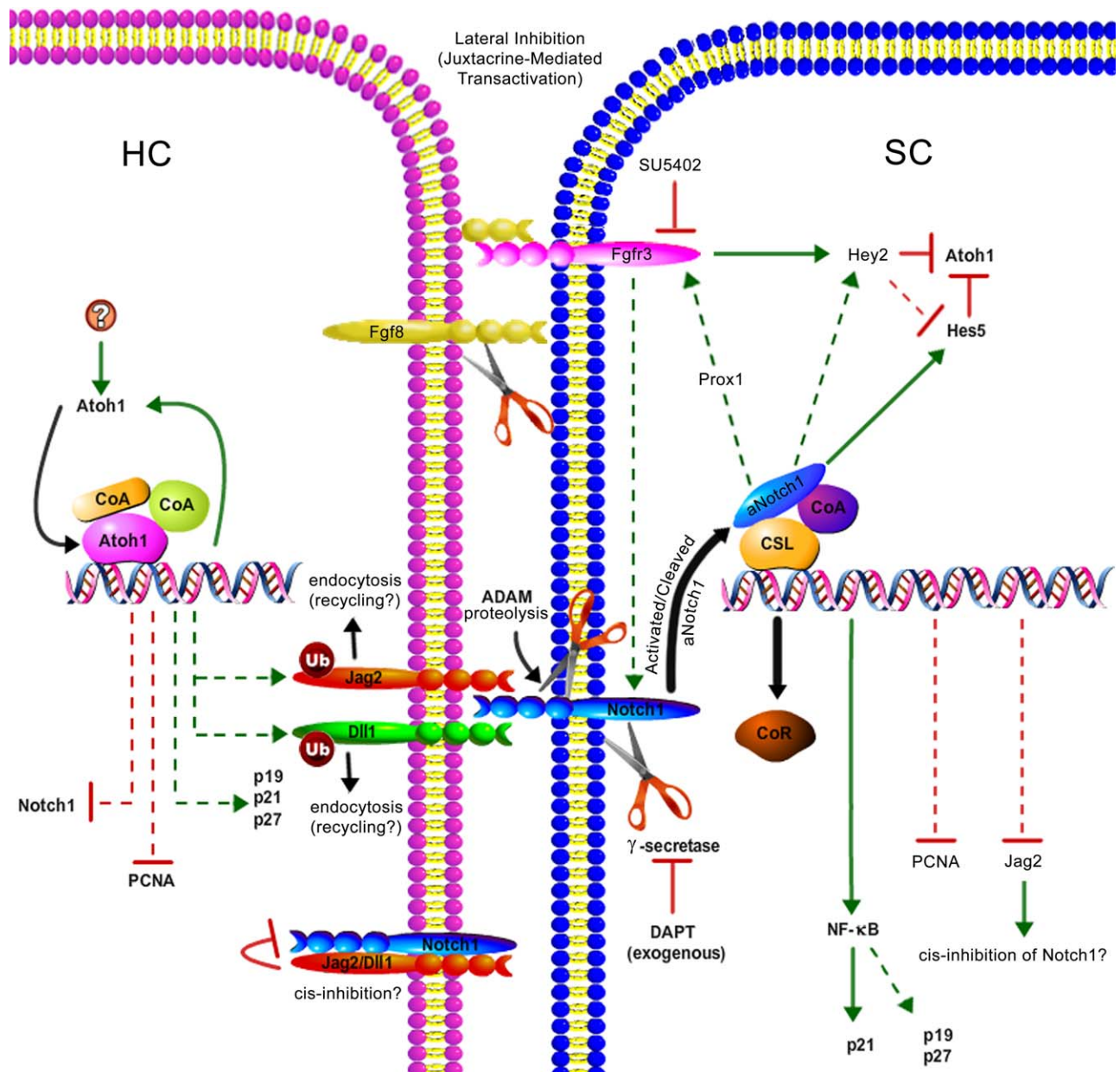


FIGURE 2. Diagram of the relationship between Notch and Fgfr3 signaling pathway. See text for details. Solid lines = direct; dashed lines = indirect; CoA, co-activator; CoR, co-repressor; Ub, ubiquitin.

myosin-VIIa (Proteus Biosciences, cat # 25-6790); FGFR3 (Santa Cruz Biotechnology, Santa Cruz, CA; cat # sc-123); Notch1 (Santa Cruz; cat # sc-6014). Nuclei were counterstained with DAPI (Invitrogen Corporation). Negative controls were performed in parallel under identical conditions and consisted of sections incubated without primary antibodies. For each treatment group, three to five cultured cochleas per day/ per antibody were analyzed. All images in this study were acquired with a Zeiss Axioplan microscope equipped with a SPOT RT3 camera

and processed with SPOT Advanced and Adobe Photoshop CS2 software.

qRT-PCR

For analysis of gene expression, qRT-PCR was conducted as previously described (Melnick et al., 2006, 2009, 2013a) on E15 + 6 and E15 + 9 control and mCMV-infected samples (n = 9/group), each consisting of four to five pooled cultured cochleas. RNA was extracted and 1 μg RNA was reverse transcribed into first strand cDNA using

ReactionReady™ First Strand cDNA Synthesis Kit: C-01 for reverse transcription (SABiosciences, Frederick, MD). The primer sets used were prevalidated to give single amplicons and purchased from SABiosciences (Frederick, MD): Atoh (Cat # PPM02976A); p19 (Cdkn2d; Cat # PPM02897A); p21 (Cdkn1a; Cat # PPM02901A); p27 (Cdkn1b; Cat # PPM02909A); Dll1 (Cat # PPM25198A); Fgf8 (PM02962A); Fgfr3 (Cat # PPM03056A); Gapdh (PPM02946A); Hes5 (Cat # PPM31391A); Hey2 (Cat # PPM30634A); Jag2 (Cat # PPM32605A); NFKb1 (PPM02930A); Notch1 (Cat # PPM04747A); PcnA (Cat # PPM03456A); Prox1 (Cat # PPM04490A). Primers were used at concentration of 0.4 microM. The cycling parameters were 95°C, 15 min; 40 cycles of (95°C, 15 sec; 55°C, 30–40 sec, and 72°C, 30 sec). Specificity of the reactions was determined by subsequent melting curve analysis. RT-PCRs of RNA (not reverse transcribed) were used as negative controls. GAPDH was used to control for equal cDNA inputs and the levels of PCR product were expressed as a function of GAPDH. The relative fold changes of gene expression between the gene of interest and GAPDH, or between the E15 + 6 and E15 + 9 control and mCMV-infected samples, were calculated by the $2^{-\Delta\Delta CT}$ method. Significant expression differences between mCMV-infected and control samples were determined by student *t* test, with $\alpha = 0.01$ and the null hypothesis of $R = 1$, where *R* is the mean relative expression ration (mCMV/control.) across the entire sample ($n = 9$). Expression ratios were log transformed before analysis to satisfy the assumption of normality.

PATHWAY AND GENE TO GENE INTERACTION ANALYSIS

Ingenuity Pathway Analysis (IPA, QIAGEN Redwood City, www.qiagen.com/ingenuity) tools were used to identify possible functional relationships between 14 probative HC/SC developmental genes (focus molecules) in E15 + 6 and E15 + 9 mCMV-infected cochleas compared with controls, using inputs of gene identifiers, \log_2 fold-changes, and *p*-values between mCMV-infected and uninfected control cochleas (see Table 1). Networks of these focus molecules were then algorithmically generated based on their connectivity, disease, and canonical pathways, and molecular and cellular functions were then ranked by score. The score associated with a particular network is the likelihood of the genes identified as differentially expressed in a network being found together by chance. Images were generated from IPA software using the canonical pathways feature, network builder feature, and the path designer tools.

Results

Based on the well-defined molecular and cellular HC/SC ontogeny in embryonic organs of Corti, we used network modeling to investigate 14 probative genes (Table 1) in the signaling pathways of lateral inhibition (Fig. 2). As

TABLE 1. Gene Expression

Gene	Days post-infection (E15 + x)					
	E15 + 6			E15 + 9		
	Δ	<i>p</i>	D	Δ	<i>p</i>	D
<i>Notch</i>	0.09	<0.001	↓	1.18	>0.01	↑
<i>Jag2</i>	0.61	<0.01	↓	26.77	<0.001	↑
<i>Dll1</i>	0.26	<0.001	↓	3.28	<0.01	↑
<i>Hes5</i>	0.22	<0.001	↓	0.48	>0.01	↓
<i>Prox1</i>	0.23	<0.001	↓	2.33	>0.01	↑
<i>p19</i>	0.18	<0.001	↓	0.58	<0.01	↓
<i>p21</i>	3.52	<0.01	↑	3.68	<0.001	↑
<i>p27</i>	0.14	<0.001	↓	0.40	<0.01	↓
<i>Pcna</i>	2.64	<0.001	↑	42.42	<0.01	↑
<i>Atoh1</i>	0.06	<0.001	↓	0.35	<0.01	↓
<i>Fgf8</i>	0.58	<0.01	↓	113.92	<0.01	↑
<i>Fgfr3</i>	0.09	<0.001	↓	1.54	>0.01	↑
<i>Hey2</i>	1.78	<0.01	↑	10.00	<0.001	↑
<i>Nfkb1</i>	0.19	<0.001	↓	0.54	<0.001	↓

Δ = mean \log_2 change across all samples ($n = 9$), i.e., the mean increase or decrease in gene expression in mCMV – treated cochleas compared to untreated cochlea controls.

P, statistical significance ($\alpha \leq 0.01$); D, direction of change, up (↑) or down (↓)

detailed in the Introduction and pictured in Figure 2, all 14 play critical roles in the gene network identified for differential HC/SC patterning. Network thinking provides the ability to simplify complex problems without losing their essential features. Because this approach is experimentally constrained and computationally accessible, it is heuristically very useful (Giuliani et al., 2014). Indeed, below we present novel emergent properties that would not be otherwise evident.

We determined the expression of 14 genes in mouse CMV (mCMV)-treated embryonic cochleas after 6 (E15 + 6) and 9 (E15 + 9) days of infection, time-points equivalent to perinatal and postnatal cochlear development, respectively (Melnick and Jaskoll, 2013). The analytical results of quantitative RT-PCR (qRT-PCR) are presented in Table 1. Remarkably, at E15 + 6, all 14 genes had significant \log_2 fold changes relative to uninfected controls, 11 downregulated and 3 upregulated. By E15 + 9, there was a very notable change: only 5 were downregulated, but 9 were upregulated, including *Notch*, *Jag2*, *Dll1*, *Fgf8*, and *Fgfr3*, consistent with the resumption of normal lateral inhibition. In typical manner, these genes may be viewed in a “signaling map” (Fig. 2) as a series of linear pathways in which initial signaling events (e.g., Atoh1, aNotch, Fgfr3), aberrant or not, progressively

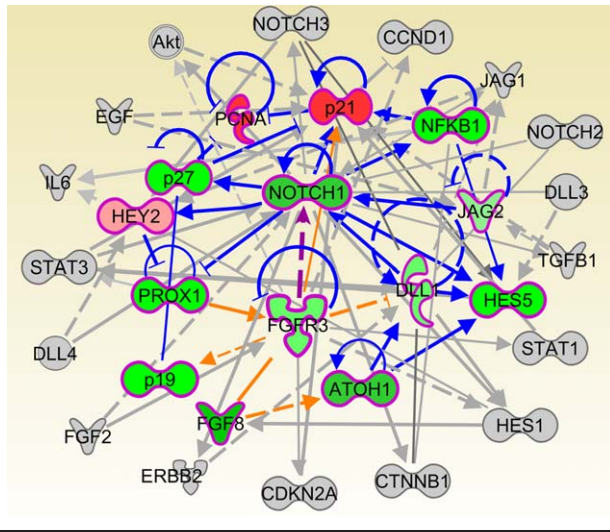


FIGURE 3. Mechanistic network analysis by IPA of the expression of 14 genes (nodes) and their known functional links (edges) in mCMV-infected E15+6 cochleas compared with controls. A small-world network showing the functional relationships between the 14 genes of interest (outlined in pink) and their nearest neighbors. The nodes are displayed using various shapes that represent the functional class of gene product and the style of the lines connecting the molecules indicates specific molecular relationships and the direction of the interaction. Notch nearest neighbors are linked by blue lines; FGFR3 nearest neighbors are linked by orange lines; and the purple arrow indicates the relationship between FGFR3 and Notch. Red-colored shapes denote upregulated genes and green colored shapes denote downregulated genes; the darker the color, the greater the change.

amplify after a sequence of Boolean choices to emerge at a variety of end-points. While this may provide a broad view, it only permits an imagined dynamic understanding.

The nonlinear complexity of living systems largely results from dynamic networks of genes rather than the sum of independent effects of individual pathways. Because the complexities of ontogenesis and teratogenesis largely emerge from complexities in the interaction of genes within and among cells, we have always to focus on the relationship between genes/pathways, rather than the genes/pathways themselves. Thus, using the qRT-PCR data (Table 1), we undertook a comprehensive functional network and pathway analysis using Ingenuity Pathway Analysis (IPA) software, as well as additional statistical approaches related to network architecture.

IPA is a Web-based software application that enables one to analyze, integrate, and understand a gene expression dataset. It is important to understand that IPA is a functional network analysis program, not a dynamic modeling or statistical analysis program. The basic design of the application is to provide insights regarding the association of a gene list (e.g., Table 1) with pathways, biologic processes and pathologies of interest. Thus, the application is upstream of statistically analyzed gene expression, and uses a robust database that is populated with the latest scientific information curated from the literature.

Structuring the largely unstructured literature, IPA decodes the gene expression data by rapidly revealing relevant functional networks. This permits progression from prior genomic statistical analysis to novel biologic insights.

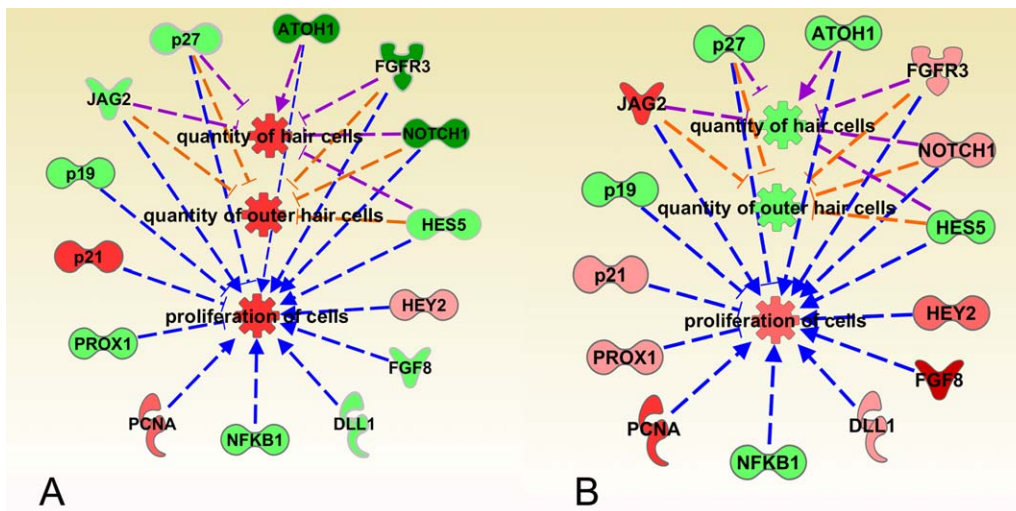


FIGURE 4. Functional analysis of 14 genes important for OC development. Network analysis using IPA and Pathway Designer showing the proteins associated with an increased number of hair cells (purple lines), an increased number of outer hair cells (orange lines) and increased cell proliferation (blue lines) on day 6 (A) and day 9 (B). Red-colored shapes denote upregulated genes and green colored shapes denote downregulated genes; the darker the color, the greater the change.

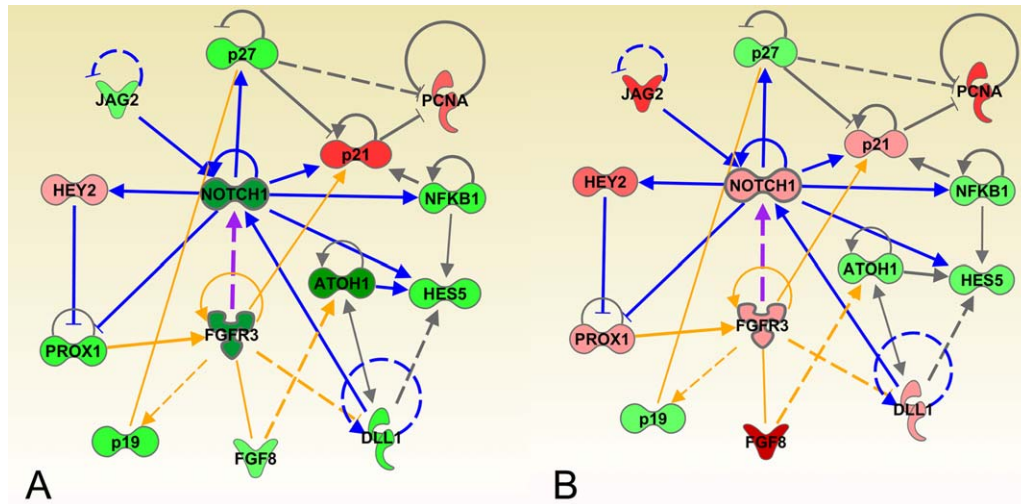


FIGURE 5. Functional network analysis of 14 genes important for OC development. Network analysis using IPA tools was conducted on the 14 differentially expressed genes and their close relationships shown in E15 + 6 (A) and E15 + 9 (B) organs of Corti. The nodes are displayed using various shapes that represent the functional class of gene product and the style of the lines connecting the molecules indicates specific molecular relationships and the direction of the interaction. Blue lines indicate direct relationships with Notch; orange lines indicate direct relationships with Fgfr3; and the purple arrow indicates the relationship between FGFR3 and Notch. Red-colored shapes denote upregulated genes and green colored shapes denote downregulated genes; the darker the color, the greater the change.

For example, using the directions of change in the gene expression dataset, IPA computes the likely effect on pathologies such as organ dysplasia and cancer. Finally, and most importantly, mathematical characterization of the IPA-identified relevant functional network allows one to further relate the molecular pathology and histopathology, by uncovering how this relationship is dependent upon network architecture.

Within a wider network context, Figure 3 illuminates the subnetwork of 14 sentinel genes (nodes) and the known functional links (edges) between them; this E15 + 6 iteration highlights nearest neighbors (colored nodes and edges, as distinguished from gray; other than node color changes consistent with Table 1 data, the E15 + 9 iteration was identical). This network appears to have a classic small world property, namely the short paths between most pairs of nodes (genes) and relatively few “long-distance” links. Furthermore, there is considerable clustering, i.e., the extent to which a gene’s nearest neighbors are also neighbors to each other, forming communities.

IPA analysis of this lateral inhibition subnetwork (Figs. 2, 3; Table 1) reveal key predictive and functional characteristics. The calculated probability at E15 + 6 that our specific qRT-PCR data set is from dysplastic organs of Corti (OC) is highly significant (Fig. 4A): *increase* in outer HCs ($p = 1.30 \times 10^{-12}$); *increase* in all HCs ($p = 8.64 \times 10^{-14}$); *increase* in general proliferation of cells ($p = 5.44 \times 10^{-9}$). By E15 + 9, there is a dramatic and significant change (Fig. 4B): *inhibition* of outer hair cells

($p = 7.92 \times 10^{-13}$); *inhibition* of all HCs ($p = 7.92 \times 10^{-13}$); *increase* in general proliferation of cells ($p = 4.35 \times 10^{-9}$). These comparative differences between key developmental time points equivalent to perinatal and postnatal cochlear development (Melnick and Jaskoll, 2013), further highlights the transient but important delay in lateral inhibition, and accounts for the increase and disorganization of differentiated HCs (Fig. 1B).

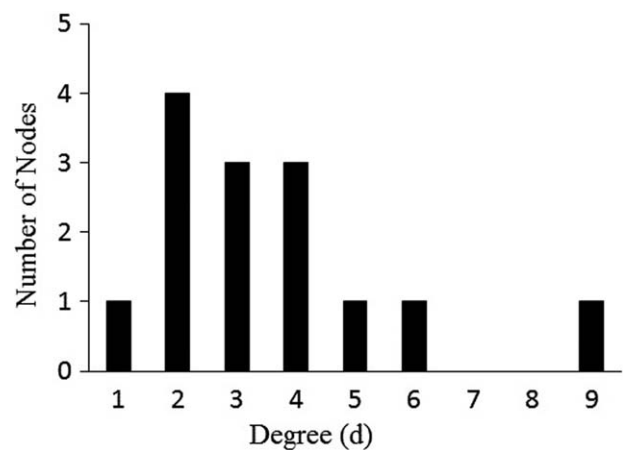


FIGURE 6. The degree (d) distribution of the network in Figure 5. For each degree, the bar represents the number of nodes (genes) with that degree. Despite the small number of genes in the subnetwork ($n = 14$), the skewed distribution is suggestive of a power law (d^{-1}) and a scale free network.

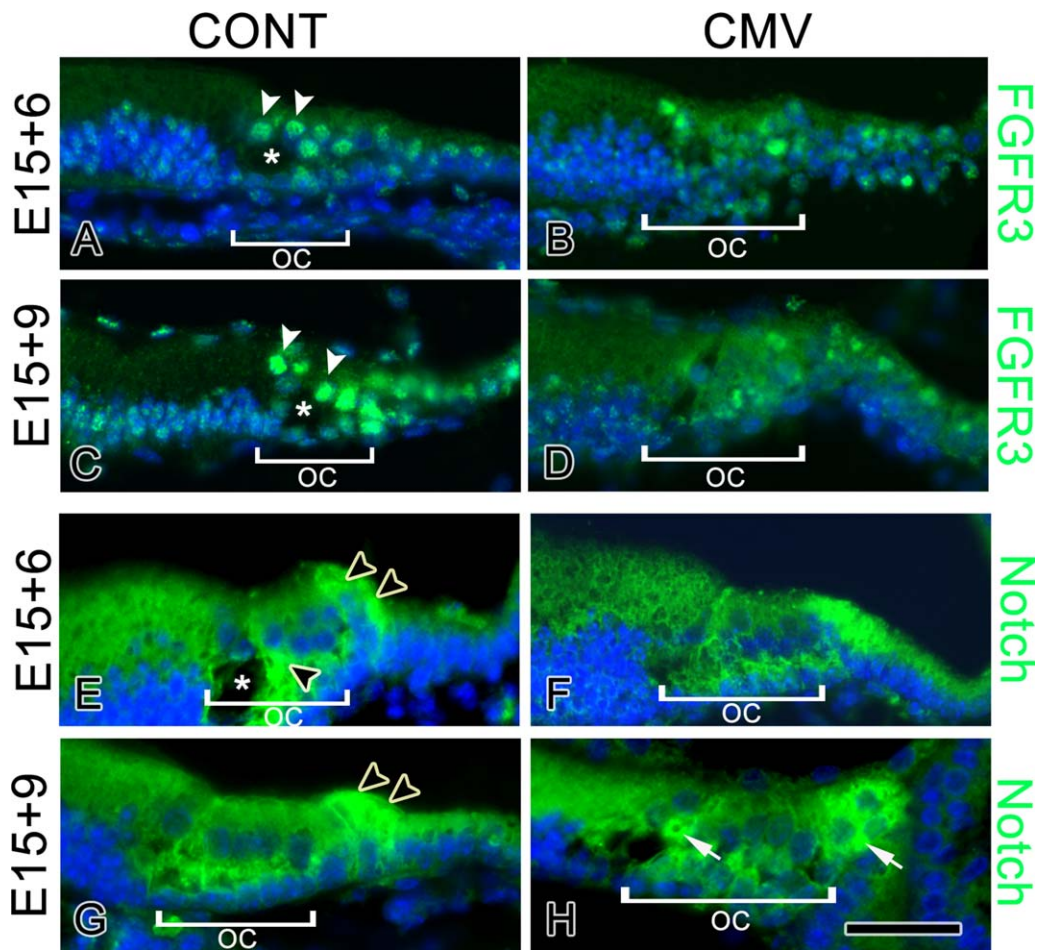


FIGURE 7. mCMV induces notable changes in the cell-specific distribution of FGFR3 and Notch proteins compared with controls. **A–D:** FGFR3 immunolocalization: In control E15+6 (A) and E15+9 (C) organs of Corti (OC, white bracket), nuclear-localized FGFR3 (white arrowheads) is found in pillar cells surrounding the tunnel of Corti (*) and in other SCs. mCMV induced a marked reduction in nuclear-localized FGFR3 in mCMV-infected E15+6 (B) and E15+9 (D) OCs compared with controls (compare B, D with A, C). **E–H:** Notch localization: In control E15+6 (E) and E15+9 (G) OCs, Notch is found in the nuclei and cytoplasm of SCs (black arrowheads), being relatively absent in HCs. mCMV infection induced a notable reduction in nuclear- and cytoplasmic-localized Notch in the densely packed and misaligned HCs and SCs on days 6 (F) and 9 (H) compared with controls (compare F, H with E, G). On day 9, Notch is also seen in a subset of HCs (white arrows) in mCMV-infected OCs. Nuclei were stained with DAPI. Scale bar = 50 μm .

Further analysis of the 14-gene subnetwork (Fig. 5) confirms that it indeed has a canonical small-world configuration (Watts and Strogatz, 1998; Mitchell, 2009): (a) short path lengths (L) between pairs of nodes (genes); (b) the degree (d) distribution (number of links in and/or out of a node) approximating a power law ($d^{-\gamma}$) typical of scale-free network (Fig. 6); (c) a mean node degree of 3.57, suggestive of the existence of hubs ($d > 5$); (d) a clustering coefficient (C) of 0.51 indicating that this is a relatively “tight-knit” community (for any genes x, y and z, if gene x is linked to genes y and z, then y and z are also linked to each other).

High degree nodes are termed hubs, a priori primary channels of information flow. There are 2 genes with a

degree (d) greater than 5 (Fig. 5): *Notch* (d = 9), *Fgfr3* (d = 6). For each hub, we calculated the average Pearson correlation coefficients (PCCs) between the hub and each respective partner for mRNA expression (as per Han et al., 2004). Hubs with mean PCCs of 0.5 or more are termed “party hubs” and those less than 0.5 are termed “date hubs”; party hubs correspond to more permanent interaction, while date hubs correspond to spatiotemporally variant, transient interactions (Han et al., 2004). Both network hubs function as date hubs, regardless of developmental time: E15 + 6: *Notch* (r = 0.19), *Fgfr3* (r = 0.14); E15 + 9: *Notch* (r = 0.31), *Fgfr3* (r = 0.19). This functional architecture remains constant even in the context of changing gene expression over time (Table 1).

Because reasonably accurate measures are problematic for most of the protein to protein interactions reflected in Figure 5 above, we have estimated the functional architecture of the two date hubs and their partner nodes with standard mRNA expression data (see Han et al., 2004). Nevertheless, it is still instructive to view the cellular distribution of both hub proteins (Fig. 7). mCMV infection induces a notable reduction in nuclear- and cytoplasmic-localized Notch and FGFR3 in the densely packed and misaligned HCs and SCs on days 6 and 9 compared with controls. What is particularly striking is that despite clear temporal gene expression changes (Table 1), there are little, if any, changes in the immunolocalization patterns between times equivalent to perinatal and postnatal mouse organ of Corti development. This suggests a more limited capacity to recover from the transient delay in lateral inhibition, a disturbing prospect for potential therapy.

Discussion

It is well-established that congenital CMV infection is the major nongenetic cause of SNHL at birth and prelingual SNHL not expressed at birth (Nance et al., 2006; Fowler, 2013). There is a striking dysplasia/hyperplasia in human and mouse CMV-infected cochlear epithelium and mesenchyme, including organ of Corti hair and supporting cells (Teissier et al., 2011; Melnick and Jaskoll, 2013; Gabrielli et al., 2013). The characteristic dramatic increase in densely packed and misaligned HCs (Fig. 1; Melnick and Jaskoll, 2013) is an abnormality known to be associated with subsequent p53-mediated HC death and progressive deafness (Chen et al., 2003; Laine et al., 2007). Presently, little is known about the cell and molecular mechanisms underlying congenital CMV SNHL. The present study was designed to provide a bit of clarity.

In short, using an in vitro embryonic mouse model of CMV-induced cochlear teratogenesis that mimics the known human pathologies and functional signaling network modeling, we demonstrate that CMV disrupts the highly ordered hair and supporting cell (HC/SC) pattern in the organ of Corti by dysregulating Notch and Fgfr3, their cognate ligands, and downstream effectors. Indeed, several novel emergent properties of the critical lateral inhibition subnetwork become apparent when the architecture of the cognate small-world signaling network is closely analyzed.

The nonlinear complexity of living systems largely results from dynamic networks of genes rather than the sum of independent effects of individual genes and pathways. Here, using gene expression data (Table 1), we undertook a comprehensive network and pathway analysis (Figs. 3–6). First, we defined a relevant molecular module, namely a discrete subnetwork whose function is separable from those of other subnetworks, a module specifically for HC/SC differentiation (Fig. 2). It is distinct by means of the initial binding of development-specific cognate ligands

to receptors, and the interaction architecture of the subnetwork (Figs. 3, 5). As Hartwell et al. (1999) note, functional modules are likely to contain components (nodes, genes) that are found in different modules at different spatiotemporal coordinates in ontogeny. This does not necessarily reflect multiple functions for a given gene, only similar function in multiple modular contexts.

Our next goal was to define the mathematical and topologic architecture of the modular subnetwork. It was immediately apparent (Fig. 3) that the subnetwork had classic small-world properties such as short paths between most node (gene) pairs, few long-distance links, and considerable clustering. Concomitantly, the calculated probability that our specific gene expression data set is from dysplastic organs of Corti is highly significant (Fig. 4A; $p < 1 \times 10^{-12}$). Furthermore, we determined that the subnetwork has a highly heterogeneous scale-free topology in which two highly linked nodes (hubs: *Notch*, *Fgfr3*) play a central role in mediating interactions among the remaining less linked nodes (Figs. 5, 6).

The scale-free topology of the lateral inhibition module has important biologic and therapeutic implications. It has been determined that the consequence of scale-free topology is the simultaneous tolerance of dysfunctional nonhub nodes and critical intolerance of dysfunctional hub nodes (Albert et al., 2000; Jeong et al., 2001). This principle can be readily seen in the present study. *Atoh1*, with few links in the network ($d = 3$), is thought to be critical for HC differentiation (Bermingham et al., 1999; Cai et al., 2013; Chonko et al., 2013). Yet, eventhough there is a dramatic downregulation ($\Delta = 0.06$; $p < 0.001$), there is “normal” differentiation of HCs (Fig. 1B). By contrast, significant downregulation ($\Delta = 0.09$; $p < 0.001$) of the SC-critical hubs *Notch* ($d = 9$) and *Fgfr3* ($d = 6$) results in considerable dysplasia of SCs (Fig. 1).

It has been shown, that hub dysfunction results in the break-up of scale-free network architecture into isolated fragments (Albert et al., 2000). Such hub vulnerability may be quite useful in cancer drug design. However, it seems quite problematic for developmental therapeutics, at least in the case of organ of Corti dysplasia. The precise enhancement of gene expression is far more difficult than blunt force inhibition. Thus, our results suggest that, going forward, vaccine-mediated prevention will ultimately be the most efficacious solution to CMV-induced congenital anomalies.

Acknowledgments

We thank Dr. Edward Mocarski for his generous gift of lacZ-tagged mCMV RM427+. T.J. and M.M. were funded by the NIH.

References

Albert R, Jeong H, Barabasi AL. 2000. Error and attack tolerance of complex networks. *Nature* 406:378–382.

- Andrei G, De Clercq E, Snoeck R. 2008. Novel inhibitors of human CMV. *Curr Opin Investig Drugs* 9:132–145.
- Bermingham NA, Hassan BA, Price SD, et al. 1999. Math1: an essential gene for the generation of inner ear hair cells. *Science* 284:1837–1841.
- Cai T, Seymour ML, Zhang H, et al. 2013. Conditional deletion of Atoh1 reveals distinct critical periods for survival and function of hair cells in the organ of Corti. *J Neurosci* 33:10110–10122.
- Cheeran MC, Lokensgard JR, Schleiss MR. 2009. Neuropathogenesis of congenital cytomegalovirus infection: disease mechanisms and prospects for intervention. *Clin Microbiol Rev* 22:99–126.
- Chen P, Zindy F, Abdala C, et al. 2003. Progressive hearing loss in mice lacking the cyclin-dependent kinase inhibitor Ink4d. *Nat Cell Biol* 5:422–426.
- Chonko KT, Jahan I, Stone J, et al. 2013. Atoh1 directs hair cell differentiation and survival in the late embryonic mouse inner ear. *Dev Biol* 381:401–410.
- Doetzlhofer A, Basch ML, Ohya T, et al. 2009. Hey2 regulation by FGF provides a Notch-independent mechanism for maintaining pillar cell fate in the organ of Corti. *Dev Cell* 16:58–69.
- Doetzlhofer A, White PM, Johnson JE, et al. 2004. In vitro growth and differentiation of mammalian sensory hair cell progenitors: a requirement for EGF and periotic mesenchyme. *Dev Biol* 272:432–447.
- Driver EC, Sillers L, Coate TM, et al. 2013. The Atoh1-lineage gives rise to hair cells and supporting cells within the mammalian cochlea. *Dev Biol* 376:86–98.
- Fowler KB. 2013. Congenital cytomegalovirus infection: audiological outcome. *Clin Infect Dis* 57(Suppl 4):S182–S184.
- Gabrielli L, Bonasoni MP, Santini D, et al. 2013. Human fetal inner ear involvement in congenital cytomegalovirus infection. *Acta Neuropathol Commun* 1:63.
- Giuliani A, Filippi S, Bertolaso M. 2014. Why network approach can promote a new way of thinking in biology. *Front Genet* 5:83.
- Han JD, Bertin N, Hao T, et al. 2004. Evidence for dynamically organized modularity in the yeast protein-protein interaction network. *Nature* 430:88–93.
- Hartwell LH, Hopfield JJ, Leibler S, Murray AW. 1999. From molecular to modular cell biology. *Nature* 402:C47–C52.
- Hayashi T, Cunningham D, Bermingham-McDonogh O. 2007. Loss of Fgfr3 leads to excess hair cell development in the mouse organ of Corti. *Dev Dyn* 236:525–533.
- Jacques BE, Dabdoub A, Kelley MW. 2012. Fgf signaling regulates development and transdifferentiation of hair cells and supporting cells in the basilar papilla. *Hear Res* 289:27–39.
- Jacques BE, Montcouquiol ME, Layman EM, et al. 2007. Fgf8 induces pillar cell fate and regulates cellular patterning in the mammalian cochlea. *Development* 134:3021–3029.
- Jahan I, Pan N, Kersigo J, Fritzsche B. 2013. Beyond generalized hair cells: molecular cues for hair cell types. *Hear Res* 297:30–41.
- Jaskoll T, Abichaker G, Htet K, et al. 2010. Cytomegalovirus induces stage-dependent enamel defects and misexpression of amelogenin, amelotin and dentin sialophosphoprotein in developing mouse molars. *Cells Tissues Organs* 192:221–239.
- Jaskoll T, Abichaker G, Jangaard N, et al. 2008a. Cytomegalovirus inhibition of embryonic mouse tooth development: a model of the human amelogenesis imperfecta phenocopy. *Arch Oral Biol* 53:405–415.
- Jaskoll T, Abichaker G, Parish SP, et al. 2008b. Cytomegalovirus induces abnormal chondrogenesis and osteogenesis during embryonic mandibular development. *BMC Dev Biol* 8:33.
- Jeong H, Mason SP, Barabási AL, Oltvai ZN. 2001. Lethality and centrality in protein networks. *Nature* 411:41–42.
- Juranic Lisnic V, Babic Cac M, Lisnic B, et al. 2013. Dual analysis of the murine cytomegalovirus and host cell transcriptomes reveal new aspects of the virus-host cell interface. *PLoS Pathog* 9:e1003611.
- Kelley MW. 2007. Cellular commitment and differentiation in the organ of Corti. *Int J Dev Biol* 51:571–583.
- Kelly MC, Chen P. 2009. Development of form and function in the mammalian cochlea. *Curr Opin Neurobiol* 19:395–401.
- Kiernan AE, Cordes R, Kopan R, et al. 2005. The Notch ligands DLL1 and JAG2 act synergistically to regulate hair cell development in the mammalian inner ear. *Development* 132:4353–4362.
- Kiernan AE. 2013. Notch signaling during cell fate determination in the inner ear. *Semin Cell Dev Biol* 24:470–479.
- Laine H, Doetzlhofer A, Mantela J, et al. 2007. p19(Ink4d) and p21(Cip1) collaborate to maintain the postmitotic state of auditory hair cells, their codeletion leading to DNA damage and p53-mediated apoptosis. *J Neurosci* 27:1434–1444.
- Melnick M, Abichaker G, Htet K, et al. 2011. Small molecule inhibitors of the host cell COX/AREG/EGFR/ERK pathway attenuate cytomegalovirus-induced pathogenesis. *Exp Mol Pathol* 91:400–410.
- Melnick M, Deluca KA, Jaskoll T. 2014. CMV-induced pathology: pathway and gene-gene interaction analysis. *Exp Mol Pathol* 97:154–165.
- Melnick M, Deluca KA, Sedghizadeh PP, Jaskoll T. 2013b. Cytomegalovirus-induced salivary gland pathology: AREG, FGF8, TNF- α , and IL-6 signal dysregulation and neoplasia. *Exp Mol Pathol* 94:386–397.
- Melnick M, Jaskoll T. 2013. An in vitro mouse model of congenital cytomegalovirus-induced pathogenesis of the inner ear cochlea. *Birth Defects Res A Clin Mol Teratol* 97:69–78.
- Melnick M, Mocarski ES, Abichaker G, et al. 2006. Cytomegalovirus-induced embryopathology: mouse submandibular salivary

- gland epithelial-mesenchymal ontogeny as a model. *BMC Dev Biol* 6:42.
- Melnick M, Phair RD, Lapidot SA, Jaskoll T. 2009. Salivary gland branching morphogenesis: a quantitative systems analysis of the Eda/Edar/NFkappaB paradigm. *BMC Dev Biol* 9:32.
- Melnick M, Sedghizadeh PP, Deluca KA, Jaskoll T. 2013a. Cytomegalovirus-induced salivary gland pathology: resistance to kinase inhibitors of the upregulated host cell EGFR/ERK pathway is associated with CMV-dependent stromal overexpression of IL-6 and fibronectin. *Herpesviridae* 4:1.
- Meloty-Kapella L, Shergill B, Kuon J, et al. 2012. Notch ligand endocytosis generates mechanical pulling force dependent on dynamin, epsins, and actin. *Dev Cell* 22:1299–1312.
- Mitchell M. 2009. *Complexity: a guided tour*. New York: Oxford University Press.
- Morton CC, Nance WE. 2006. Newborn hearing screening—a silent revolution. *N Engl J Med* 354:2151–2164.
- Murata J, Ikeda K, Okano H. 2012. Notch signaling and the developing inner ear. *Adv Exp Med Biol* 727:161–173.
- Murata J, Ohtsuka T, Tokunaga A, et al. 2009. Notch-Hes1 pathway contributes to the cochlear prosensory formation potentially through the transcriptional down-regulation of p27Kip1. *J Neurosci Res* 87:3521–3534.
- Musse AA, Meloty-Kapella L, Weinmaster G. 2012. Notch ligand endocytosis: mechanistic basis of signaling activity. *Semin Cell Dev Biol* 23:429–436.
- Nance WE, Lim BG, Dodson KM. 2006. Importance of congenital cytomegalovirus infections as a cause for pre-lingual hearing loss. *J Clin Virol* 35:221–225.
- Pan W, Jin Y, Stanger B, Kiernan AE. 2010. Notch signaling is required for the generation of hair cells and supporting cells in the mammalian inner ear. *Proc Natl Acad Sci U S A* 107:15798–15803.
- Puligilla C, Feng F, Ishikawa K, et al. 2007. Disruption of fibroblast growth factor receptor 3 signaling results in defects in cellular differentiation, neuronal patterning, and hearing impairment. *Dev Dyn* 236:1905–1917.
- Schwegmann A, Brombacher F. 2008. Host-directed drug targeting of factors hijacked by pathogens. *Sci Signal* 1:re8.
- Szarama KB, Stepanyan R, Petralia RS, et al. 2012. Fibroblast growth factor receptor 3 regulates microtubule formation and cell surface mechanical properties in the developing organ of Corti. *Bioarchitecture* 2:214–219.
- Schleiss MR. 2011. Congenital cytomegalovirus infection: molecular mechanisms mediating viral pathogenesis. *Infect Disord Drug Targets* 11:449–465.
- Schleiss MR, McVoy MA. 2004. Overview of congenitally and perinatally acquired cytomegalovirus infections: recent advances in antiviral therapy. *Expert Rev Anti Infect Ther* 2:389–403.
- Teissier N, Delezoide AL, Mas AE, et al. 2011. Inner ear lesions in congenital cytomegalovirus infection of human fetuses. *Acta Neuropathol* 122:763–774.
- Van de Water TR, Represa J. 1991. Tissue interactions and growth factors that control development of the inner ear: Neural tube-otic anlage interaction. *Ann N Y Acad Sci* 630:116–128.
- Van de Water TR, Ruben RJ. 1971. Organ culture of the mammalian inner ear. *Acta Otolaryngol* 71:303–312.
- Watts DJ, Strogatz SH. 1998. Collective dynamics of ‘small-world’ networks. *Nature* 393:440–442.
- Xu H, Chen L, Baldini A. 2007. In vivo genetic ablation of the periotic mesoderm affects cell proliferation survival and differentiation in the cochlea. *Dev Biol* 310:329–340.